Phase transitions and generalized biorthogonal polarization in non-Hermitian systems

Elisabet Edvardsson,[1,*] Flore K. Kunst,[2] Tsuneya Yoshida,[3] and Emil J. Bergholtz[1,†]
[1]*Department of Physics, Stockholm University, AlbaNova University Center, 106 91 Stockholm, Sweden*
[2]*Max-Planck-Institut für Quantenoptik, Hans-Kopfermann-Straße 1, 85748 Garching, Germany*
[3]*Department of Physics, University of Tsukuba, Ibaraki 305-8571, Japan*

(Received 28 June 2020; accepted 15 September 2020; published 8 October 2020)

Non-Hermitian (NH) Hamiltonians can be used to describe dissipative systems, notably including systems with gain and loss, and are currently intensively studied in the context of topology. A salient difference between Hermitian and NH models is the breakdown of the conventional bulk-boundary correspondence, invalidating the use of topological invariants computed from the Bloch bands to characterize boundary modes in generic NH systems. One way to overcome this difficulty is to use the framework of biorthogonal quantum mechanics to define a biorthogonal polarization, which functions as a real-space invariant signaling the presence of boundary states. Here, we generalize the concept of the biorthogonal polarization beyond the previous results to systems with any number of boundary modes and show that it is invariant under basis transformations as well as local unitary transformations. Additionally, we focus on the anisotropic Su-Schrieffer-Heeger chain and study gap closings analytically. We also propose a generalization of a previously developed method with which to find all the bulk states of the system with open boundaries to NH models. Using the exact solutions for the bulk and boundary states, we elucidate genuinely NH aspects of the interplay between the bulk and boundary at the phase transitions.

DOI: 10.1103/PhysRevResearch.2.043046

I. INTRODUCTION

One of the fundamental postulates of quantum mechanics is the assumption that observables are described by Hermitian operators, which ensures realness of the measured eigenvalues. This, however, fails to take into account that in reality systems typically interact with the environment, giving rise to dissipation and other nonequilibrium phenomena. An effective approach to describe such open systems is by making use of *non-Hermitian* (NH) operators. The study of NH Hamiltonians has in recent years become increasingly popular and finds applications in classical systems, e.g., in optics [1–11], electric circuits [12–18], and topological mechanical metamaterials [19–22], and also in quantum systems, such as quasiparticles with finite lifetimes in heavy-fermion systems [23–25] and material junctions [26]. Recently, there has been an increasing focus on studying the topological properties of such NH systems [27], which have been studied both theoretically [28–54] and experimentally [55–65].

Alleviating the Hermiticity condition may introduce effects that, at first glance, seem surprising or unintuitive, such as the possible breakdown of the conventional bulk-boundary correspondence (BBC) [30–38]. This phenomenon is accompanied by the so-called NH skin effect, which refers to the piling up of bulk states at the boundaries [37], as well as the appearance of exceptional points (EPs), which are degeneracies at which the geometric multiplicity is smaller than the algebraic multiplicity, whose order scales with system size [38]. The breakdown of the conventional BBC as well as the emergence of the NH skin effect has been experimentally verified in mechanical systems [20,21], topoelectrical circuits [16], and optical [61] systems. This phenomenology has also been suggested to be of practical use in sensors whose sensitivity increases exponentially with the size of the system [66].

Crucially, when the conventional BBC is broken, it is no longer possible to directly use topological invariants derived from the Bloch Hamiltonian to characterize the topological phase of the system or to predict the presence of boundary states. In Refs. [30,31] several of the authors of this work proposed an alternative BBC to remedy this breakdown called the *biorthogonal bulk-boundary correspondence*, which finds its basis in biorthogonal quantum mechanics [67]. Explicitly using the fact that the left and right eigenstates of an NH Hamiltonian are generally different and nonorthogonal, the biorthogonal BBC considers the combination of these eigenstates to accurately predict the localization of boundary modes as well as gap closings in the open-boundary-condition (OBC) spectrum [30].

Indeed, one of the central results of Ref. [30] is the introduction of the *biorthogonal polarization*

$$\mathcal{P} = 1 - \lim_{N\to\infty} \frac{1}{N} \langle \psi_L | \sum_n n \hat{\Pi}_n | \psi_R \rangle, \tag{1}$$

where $\hat{\Pi}_n$ is the projection operator onto the nth unit cell of the lattice with OBCs, N is the total number of unit cells,

*elisabet.edvardsson@fysik.su.se
†emil.bergholtz@fysik.su.se

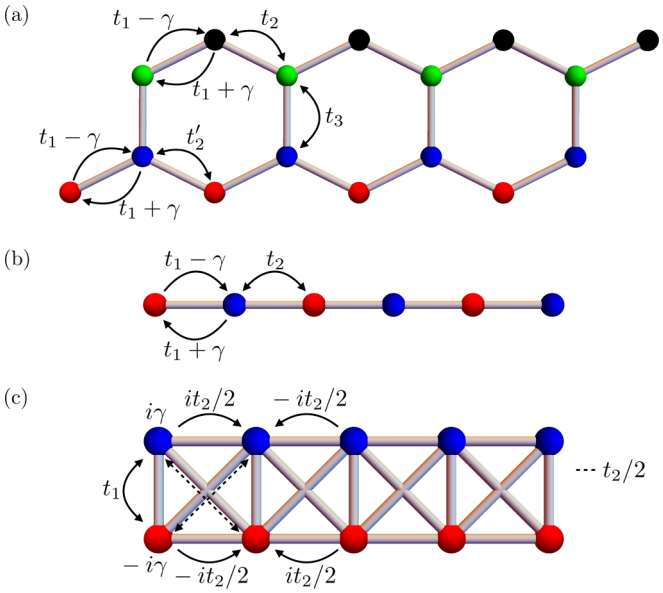

FIG. 1. Hamiltonian for (a) the two-leg ladder, (b) the anisotropic SSH chain, and (c) the Lee model. The differently colored sites refer to different sublattice sites.

and ψ_L and ψ_R are the left and right eigenstates, respectively, of the boundary mode. This predicts the presence ($\mathcal{P}=1$) or absence ($\mathcal{P}=0$) of a boundary mode on each boundary in quasi-one-dimensional systems, i.e., systems with OBCs in one direction, and can thus be interpreted as a real-space invariant. In this paper, we generalize this quantity to quasi-one-dimensional systems with *any* number of boundary modes and show with an example that its value corresponds exactly to the number of boundary modes on the boundaries. Additionally, we show that the polarization is invariant under gauge transformations as well as unitary transformations that are local, thus corroborating the invariance of the polarization.

We also present a study of the OBC properties of the anisotropic Su-Schrieffer-Heeger (SSH) chain [see Fig. 1(b)] by studying the gap closings, which so far mainly have been studied numerically, as well as analytical solutions for all the bulk states. By making use of analytical results from Refs. [30,38] for the periodic-boundary-condition (PBC) and OBC cases, we study the behaviors of the band-gap closing in the PBC and OBC spectra and find that they scale differently with system size. Additionally, we show that the method in Ref. [69] for finding all bulk-state solutions analytically can be extended to the NH realm. Whereas in Hermitian systems this method relies on a *spectral mirror symmetry* in the Bloch spectrum relating the eigenvalues at k to the eigenvalues at $-k$, here, we find that this symmetry needs to be present only in the OBC spectrum, i.e., $E_{\mathrm{OBC}}(k)=E_{\mathrm{OBC}}(-k)$, whereas it may be absent in the Bloch spectrum. By taking a closer look at these solutions at the gap closings, we can show that they are equivalent to the boundary states up to a twist, similar to what was done in Ref. [68], thus proving that the gap, indeed, disappears.

This paper is organized as follows: In Sec. II, we introduce the generalized biorthogonal polarization and discuss its properties. This is followed by a thorough study of the anisotropic SSH chain in Sec. III. Last, we conclude with a discussion in Sec. IV.

II. THE BIORTHOGONAL POLARIZATION

In this section, we define, generalize, and discuss the properties of the biorthogonal polarization, which was originally introduced in Ref. [30] for quasi-one-dimensional models with a maximum of one boundary state on each boundary [see Eq. (1)]. We note that throughout this section we assume models with OBCs, where the boundaries have codimension 1.

A. Basic properties of the biorthogonal polarization

We define the following generalized biorthogonal polarization operator:

$$\hat{P}=\mathbb{1}-\lim_{N\to\infty}\frac{1}{N}\sum_{n=1}^{N}n\hat{\Pi}_n, \tag{2}$$

where N is the total number of unit cells in the system and $\hat{\Pi}_n=\sum_m|e_{nm}\rangle\langle e_{nm}|$, with $|e_{nm}\rangle\equiv c_{nm}^\dagger|0\rangle$, is a projection operator that projects onto the nth unit cell with m labeling the internal degrees of freedom inside the unit cell n. From this we define the biorthogonal polarization $\mathcal{P}$ as

$$\mathcal{P}=\mathrm{tr}[P_{\alpha\beta}], \tag{3}$$

where the trace is over the matrix $P_{\alpha\beta}$ with matrix elements

$$P_{\alpha\beta}=\langle\psi_{\alpha L}|\hat{P}|\psi_{\beta R}\rangle, \tag{4}$$

where $|\psi_{\alpha R/L}\rangle$ labels the right/left boundary modes. For a system with M edge modes, we thus find

$$\mathcal{P}=M-\lim_{N\to\infty}\frac{1}{N}\sum_{\alpha=1}^{M}\langle\psi_{\alpha L}|\left(\sum_{n=1}^{N}n\hat{\Pi}_n\right)|\psi_{\alpha R}\rangle, \tag{5}$$

where we see immediately that we retrieve Eq. (1) for $M=1$.

The biorthogonal polarization $\mathcal{P}$ takes integer values $\mathcal{P}\in\mathbb{Z}$. This was explained in Ref. [30], and we summarize the argument here for the sake of completion. Assume a lattice model with a broken unit cell at one of the boundaries, by which we mean a model where the unit cell at one end of the chain misses one or more sublattice sites, such that each boundary state contained in M always exists regardless of the choice of parameters [70], where the parameter choices determine the boundary on which the state is localized. Additionally, assume that the boundary states are chosen in such a way that they are biorthogonal to each other, i.e.,

$$\langle\psi_{\alpha L}|\psi_{\beta R}\rangle=\delta_{\alpha\beta}\langle\psi_{\alpha L}|\psi_{\alpha R}\rangle=\delta_{\alpha\beta}. \tag{6}$$

Let us focus on what happens when a boundary state is localized to unit cell $n=1$. In this case, the limit in Eq. (5) goes to zero. Similarly, if the state is localized to unit cell $n=N$, the limit goes to 1. Therefore, each localized state contributes either a 0 or a 1 to $\mathcal{P}$, and $\mathcal{P}$ must thus be quantized.

Another consequence of the above explanation is that the biorthogonal polarization $\mathcal{P}$ of a system with a broken unit cell tells us how many of the boundary states in the system are localized to the boundary at $n=1$ (while $M-\mathcal{P}$ tells us how many boundary states are localized at $n=N$). Crucially,

$\mathcal{P}$ is also a relevant quantity for systems without a broken unit cell. In this case, one can think of the lattice as having mirror symmetry up to local permutations of the internal degrees of freedom in a unit cell, such that each boundary state localized to $n = 1$ has a "mirror-symmetric" partner localized to $n = N$. In other words, this means that if one finds p boundary states on the boundary $n = 1$ ($n = N$) in the case of a lattice with a broken unit cell, one would find p (zero) boundary states on both boundaries in the case of unbroken unit cells. Therefore, for a lattice with no broken unit cells, the value of $\mathcal{P}$ corresponds to the total number of boundary states on either boundary, and $\mathcal{P} = 0$ when there are no boundary states. In the following, we always assume that the unit cell is unbroken unless otherwise specified.

To illustrate this in more detail, we consider the example of a two-leg ladder, as shown in Fig. 1(a). The Hamiltonian reads

$$H = H_H + H_{\mathrm{AH}}, \tag{7}$$

with

$$H_H = t_1 \sum_{n,l} c^\dagger_{n,l,A} c_{n,l,B} + t_2 \sum_n c^\dagger_{n+1,a,A} c_{n,a,B} + t_2' \sum_n c^\dagger_{n+1,b,A} c_{n,b,B} + t_3 \sum_n c^\dagger_{n,a,A} c_{n,b,B} + \mathrm{H.c.} \tag{8}$$

and

$$H_{\mathrm{AH}} = \gamma \sum_{n,l} [c^\dagger_{n,l,A} c_{n,l,B} - \mathrm{H.c.}], \tag{9}$$

where $c^\dagger_{n,l,\alpha}$ ($c_{n,l,\alpha}$) creates (annihilates) a state at sublattice $\alpha \in \{A, B\}$ in unit cell n with channel $l = a, b$. When $t_3 = 0$, we obtain two decoupled anisotropic SSH chains [see Fig. 1(b)]. We note that H_H is Hermitian and that H_{AH} is anti-Hermitian, such that the Hamiltonian H is non-Hermitian. As each individual SSH chain may host at most one end mode at each end, we may find two, one, or zero end modes on each of the boundaries of the two-leg ladder depending on the choice of parameters. In Figs. 2(a) and 2(b), we plot the band spectrum and the biorthogonal polarization, respectively, for different system sizes. We see that the number of end modes varies as a function of t_1, where $\mathcal{P}$ [see Fig. 2(b)] accurately predicts the number of zero-energy end states in accordance with Fig. 2(a). Indeed, the biorthogonal polarization jumps at those values of t_1 at which the band gap closes. We note that the biorthogonal polarization approaches a step function as we increase the system size as advertised.

B. Properties of the biorthogonal polarization

Here, we discuss several interesting properties of the biorthogonal polarization. First, $\mathcal{P}$ is gauge invariant: Assuming that the edge modes $|\phi_{\alpha,R}\rangle$ are degenerate and that there is an invertible matrix V such that

$$|\psi_{\alpha R}\rangle = \sum_{\alpha'} |\phi_{\alpha' R}\rangle V_{\alpha'\alpha} \tag{10}$$

and that both ϕ and ψ are normalized according to

$$\langle \psi_{\alpha L} | \psi_{\beta R} \rangle = \langle \phi_{\alpha L} | \phi_{\beta R} \rangle = \delta_{\alpha\beta}, \tag{11}$$

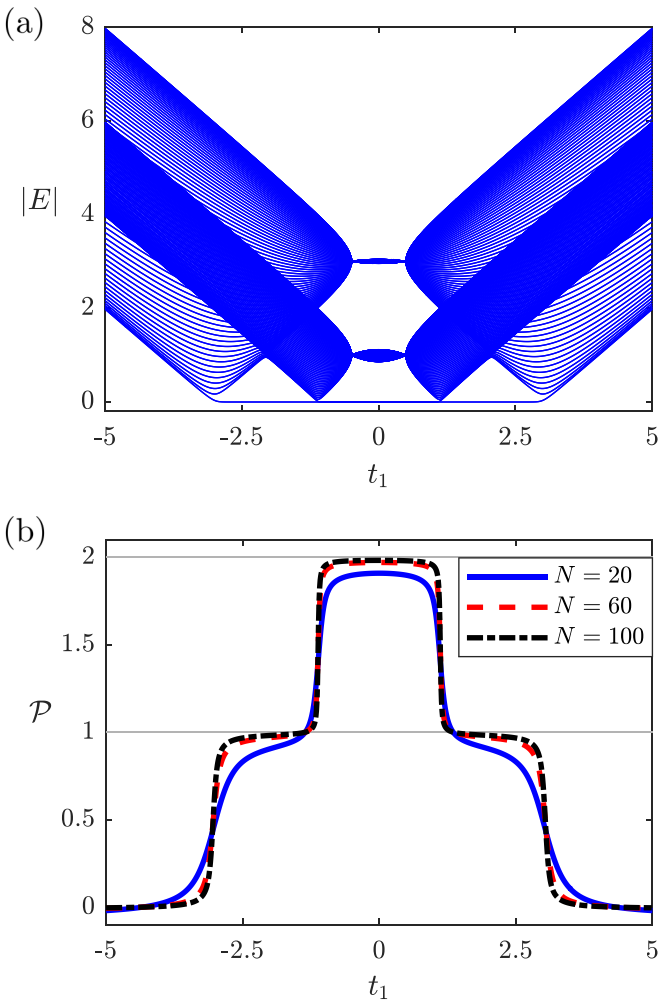

FIG. 2. (a) Absolute value of the energy eigenvalues and (b) the biorthogonal polarization for the two-leg ladder [see Fig. 1(a)] with $t_2 = 3$, $t_2' = 1$, $t_3 = 0.1$, and $\gamma = 0.5$. The eigenvalues are computed for $N = 80$ unit cells, and the polarization is computed for the values $N = 20$ (blue solid line), 60 (red dashed line), and 100 (black dash-dotted line) unit cells.

the corresponding left eigenvector can be written as

$$\langle \psi_{\alpha L}| = \sum_{\alpha'} V^{-1}_{\alpha\alpha'} \langle \phi_{\alpha' L}|, \tag{12}$$

where $V^{-1}_{\alpha\alpha'} \equiv [V^{-1}]_{\alpha\alpha'}$. This gives

$$\begin{aligned} &\frac{1}{N} \sum_{\alpha=1}^{M} \langle \psi_{\alpha L}| \left(\sum_n n \hat{\Pi}_n \right) |\psi_{\alpha R}\rangle \\ &= \frac{1}{N} \sum_{\alpha,\beta,\gamma=1}^{M} V^{-1}_{\alpha\beta} \langle \phi_{\beta L}| \left(\sum_n n \hat{\Pi}_n \right) |\phi_{\gamma R}\rangle V_{\gamma\alpha} \\ &= \frac{1}{N} \sum_{\beta=1}^{M} \langle \phi_{\beta L}| \left(\sum_n n \hat{\Pi}_n \right) |\phi_{\beta R}\rangle, \end{aligned} \tag{13}$$

and we thus find that the polarization is invariant under the change of basis. This is an important characteristic of $\mathcal{P}$ because it means that regardless of the choice one makes for

representing $|\psi_{\alpha R/L}\rangle$, one would always find the same result for $\mathcal{P}$.

Another interesting property of the biorthogonal polarization is that it is invariant under unitary transformations of the Hamiltonian that are local in the sense that they act locally on all unit cells in the same way. Indeed, suppose that we have two Hamiltonians H and $\tilde{H}$ that are related via

$$\tilde{H} = U_N^\dagger H U_N, \tag{14}$$

where U_N is a unitary operator of the form $U_N = \mathbb{1}_N \otimes U$, with $\mathbb{1}_N$ being the N-dimensional identity matrix and U being a $d \times d$ matrix, where d is the total number of degrees of freedom in a unit cell in the system described by H. Next, suppose $|\psi_{R/L}\rangle$ is the right/left eigenvector of H with eigenvalue E; then $U^\dagger|\psi_{R/L}\rangle$ is a right/left eigenvector of $\tilde{H}$ with eigenvalue E. This means that the biorthogonal polarization $\tilde{\mathcal{P}}$ of $\tilde{H}$ is given by

$$\tilde{\mathcal{P}} = M - \lim_{N\to\infty} \frac{1}{N} \sum_{\alpha=1}^{M} \langle \psi_{L,\alpha}| U \sum_n n \hat{\Pi}_n U^\dagger |\psi_{R,\alpha}\rangle, \tag{15}$$

where $\hat{\Pi}_n$ projects the states onto unit cell n such that it can be written as $\hat{\Pi}_n = J_n \otimes \mathbb{1}_d$, where J_n is an N-dimensional matrix with zeros everywhere except at position (n, n), where we have a 1. Since U_N and $\hat{\Pi}_n$ have the same block structure, they must commute, and therefore,

$$\tilde{\mathcal{P}} = \mathcal{P}. \tag{16}$$

The biorthogonal polarization is thus indeed invariant under this type of unitary transformation. To illustrate the implications of this equality, we consider the anisotropic SSH chain [30] and the Lee model [35] shown in Figs. 1(b) and 1(c), respectively. These two models have the following Bloch Hamiltonians:

$$\begin{aligned} H_{\text{Bloch}}^{\text{SSH}} &= (t_1 + t_2 \cos k,\ t_2 \sin k + i\gamma,\ 0) \cdot \boldsymbol{\sigma}, \\ H_{\text{Bloch}}^{\text{Lee}} &= (t_1 + t_2 \cos k,\ 0,\ t_2 \sin k + i\gamma) \cdot \boldsymbol{\sigma}, \end{aligned} \tag{17}$$

where $\boldsymbol{\sigma}$ is the vector of Pauli matrices. We immediately see that these Hamiltonians can be related via

$$H_{\text{Bloch}}^{\text{Lee}} = U^\dagger H_{\text{Bloch}}^{\text{SSH}} U, \tag{18}$$

where U is given by

$$U = \frac{1}{\sqrt{2}} \begin{pmatrix} 1 & i \\ i & 1 \end{pmatrix}. \tag{19}$$

It is straightforward to show that the Hamiltonians for the anisotropic SSH chain and the Lee model under OBCs are also related by a unitary transformation,

$$H_N^{\text{Lee}} = U_N^\dagger H_N^{\text{SSH}} U_N, \tag{20}$$

where U_N is defined as above and H_N^{SSH} and H_N^{Lee} are the OBC Hamiltonians with N unit cells for the NH SSH and Lee models, respectively. Therefore, the biorthogonal polarizations of these systems are equivalent. A complementary consequence of the relation in Eq. (20) is that the spectra of H_N^{SSH} and H_N^{Lee} are identical, while their eigenstates are equal up to permutations inside the unit cell determined by U. Therefore, the exact solutions for the zero-energy end states of the anisotropic SSH chain found in Ref. [30], which are discussed in more detail in the next section, are also relevant for Lee's model.

III. BULK STATES AND GAP CLOSINGS

In this section, we study the anisotropic SSH chain in more detail through explicit analytical solutions. It was previously shown that this model breaks conventional BBC and thus displays a spectral instability as well as the non-Hermitian skin effect [30,37]. Here, we make use of analytical solutions to study the gap closings of the spectrum in more detail. Additionally, we show that the method developed in Ref. [69] for finding all bulk states in the presence of a spectral mirror symmetry can be generalized to this NH model.

A. Closing of the energy gap

We consider the Bloch Hamiltonian for the anisotropic SSH chain in Eq. (17) with the energy eigenvalues

$$E_\pm^{\text{PBC}}(k) = \pm\sqrt{t_1^2 + t_2^2 - \gamma^2 + 2t_1 t_2 \cos(k) + 2it_2\gamma \sin(k)} \tag{21}$$

and (unnormalized) eigenstates

$$\psi_{R,\pm}(k) = \begin{pmatrix} t_1 + \gamma + t_2 e^{-ik} \\ E_\pm^{\text{PBC}}(k) \end{pmatrix}, \tag{22}$$

$$\psi_{L,\pm}(k) = \begin{pmatrix} t_1 - \gamma + t_2 e^{-ik} \\ [E_\pm^{\text{PBC}}(k)]^* \end{pmatrix}. \tag{23}$$

Here, we include the label PBC for the eigenvalues, indicating that if we parametrize k such that $k = 2\pi j/N$ for $j = 0, 1, \ldots, N-1$ in $E_\pm^{\text{PBC}}(k)$, we find the band spectrum for the model with PBCs.

Taking OBCs with a broken unit cell at one boundary, we find that one zero-energy end state appears. In Ref. [30], it is shown that this end state is captured by the exact solution

$$|\psi_{R/L}\rangle = \mathcal{N}_{R/L} \sum_{n=1}^{N} r_{R/L}^n c_{n,A}^\dagger |0\rangle, \tag{24}$$

with $\mathcal{N}_{R/L}$ being the normalization and $r_{R/L} = (t_1 \mp \gamma)/t_2$. This end state is delocalized when $|r_R r_L| = 1$ [30], which can also be seen from the biorthogonal polarization in Eq. (1), where $\mathcal{P}$ changes values when $|r_R r_L| = 1$. Therefore, we expect the bulk-band gap of the OBC spectrum to close at this point. To see this, we compute the eigenvalues of the OBC system from the PBC spectrum by applying a shift in k in the latter, similar to the shift in Refs. [37,38], i.e.,

$$k \to k - i \ln\left(\frac{\sqrt{t_1 - \gamma}}{\sqrt{t_1 + \gamma}}\right), \tag{25}$$

such that the OBC spectrum reads

$$\begin{aligned} E_\pm^{\text{OBC}}(k) &= E_\pm^{\text{PBC}}\left[k - i \ln\left(\frac{\sqrt{t_1 - \gamma}}{\sqrt{t_1 + \gamma}}\right)\right] \\ &= \pm\sqrt{t_1^2 + t_2^2 - \gamma^2 + 2t_2\sqrt{t_1 - \gamma}\sqrt{t_1 + \gamma}\cos(k)}. \end{aligned} \tag{26}$$

We note that $|r_R r_L| = 1$ yields $t_2 = \pm\sqrt{t_1^2 - \gamma^2}$ for $|t_1| > |\gamma|$, such that $E_\pm^{\text{OBC}}(k) = 0$ for $k = 0, \pi$, depending on the

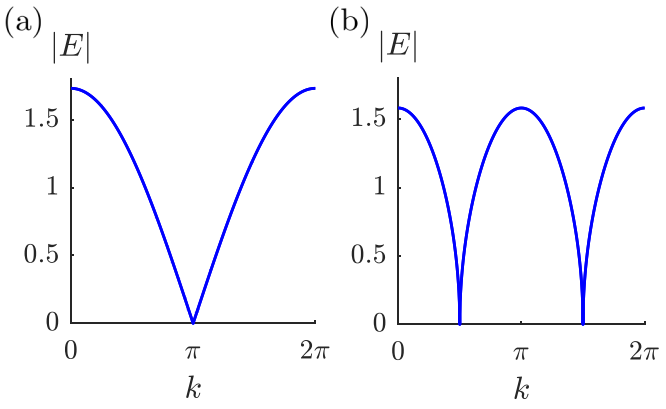

FIG. 3. The lowest bulk energy bands of the OBC spectrum [see Eq. (26)] with a broken unit cell after taking the absolute value for $t_1 = 1$ and (a) $t_2 = \sqrt{3}/2$ and $\gamma = 0.5$ and (b) $t_2 = \sqrt{5}/2$ and $\gamma = 1.5$. The former case corresponds to the spectrum being real, while the latter corresponds to the spectrum being complex. Notably, the spectrum in (b) also exhibits the genuinely non-Hermitian feature of a nonanalytic (square-root) dispersion.

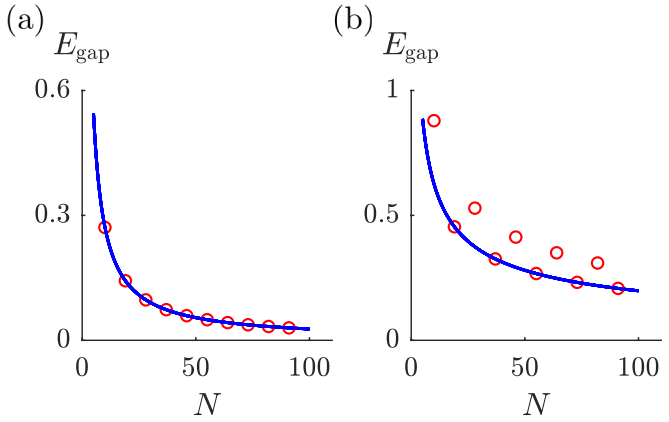

FIG. 4. Energy gap closing $E_{\rm gap}$, which corresponds to the lowest nonzero energy bulk band in the absolute value spectrum in the OBC spectrum with a broken unit cell as a function of N for (a) $t_2^2 = t_1^2 - \gamma^2$ and (b) $t_2^2 = \gamma^2 - t_1^2$. The red dots are analytically computed from Eq. (26), whereas the blue lines correspond to the lines $E_{\rm gap} = t_2\pi/N$ and $E_{\rm gap} = t_2\sqrt{\pi/N}$ in the left and right panels, respectively. We see that there is good agreement between the actual gap sizes (red dots) and the approximated result (blue line).

sign in front of the square root. Similarly, when $|t_1| < |\gamma|$, $|r_R r_L| = 1$ yields $t_2 = \pm\sqrt{\gamma^2 - t_1^2}$, and we find $E_\pm^{\rm OBC}(\pi/2) = E_\pm^{\rm OBC}(3\pi/2) = 0$. This means that the gap closes at these parameters for $k = 0, \pi$ or $k = \pi/2$ and $3\pi/2$, respectively, as illustrated in Fig. 3. Furthermore, we see that the PBC spectrum $E_\pm^{\rm PBC}(k)$ remains gapped for all k when $|r_R r_L| = 1$. This is in full agreement with the previous statement that this model features a spectral instability [30].

Performing a series expansion of $E_\pm^{\rm OBC}(k)$ at $t_2 = \pm\sqrt{t_1^2 - \gamma^2}$ and $t_2 = \pm\sqrt{\gamma^2 - t_1^2}$ around the points $k = \pi$ and $k = \pi/2$, respectively, we find that the gap closes as $E_{\rm gap} \sim 1/N$ and $E_{\rm gap} \sim 1/\sqrt{N}$, respectively (see the blue lines in Fig. 4), where $E_{\rm gap}$ is determined by first taking the absolute value of the energy spectrum and subsequently computing the smallest energy above zero. The latter result is particularly interesting as this type of scaling typically does not occur in Hermitian systems, and in this case it happens when the eigenvalues are complex. We can understand this difference between Hermitian and NH systems by noting that in a Hermitian system the bulk energies are essentially the same under PBCs and OBCs up to possible boundary states. Under PBCs, the energies are periodic functions of $k \sim 1/N$ and have Fourier expansions in k. This means that the gap closes at least as fast as $1/N$. This argument clearly fails in the NH case in the absence of a conventional BBC.

B. Exact bulk-state solutions

In Ref. [69], it was shown by some of the authors of this paper that it is possible to find all bulk-state solutions for a large family of d-dimensional lattice models with OBCs when the spectrum has mirror symmetry, i.e., $E(k_\perp, \mathbf{k}_\parallel) = E(-k_\perp, \mathbf{k}_\parallel)$, where $k_\perp$ is the momentum in the direction of the open boundary and $\mathbf{k}_\parallel$ is the crystal momentum in the periodic directions. Here, we propose a generalization of this method to the NH realm by specifically focusing on the anisotropic SSH chain.

We start by observing that even though the eigenvalues for the PBC spectrum in Eq. (21) are not symmetric under inversion symmetry, i.e., $E_\pm^{\rm PBC}(k) \neq E_\pm^{\rm PBC}(-k)$, the eigenvalues in the case of OBC do display this spectral symmetry, i.e., $E_\pm^{\rm OBC}(k) = E_\pm^{\rm OBC}(-k)$, and we should thus be able to adopt the method developed in Ref. [69] to find the eigenstates also in this NH setting even in the presence of the NH skin effect. We note that such a distinction between the PBC and OBC spectra does not exist in the Hermitian case because the spectra would be essentially identical.

To find the right eigenstates, we start by considering a periodic chain with $2N$ unit cells. From Ref. [69], we know that the state in the nth unit cell of a *Hermitian* system reads

$$\Psi_{R,\pm}(k, n) = e^{ikn}\psi_{R,\pm}(k), \tag{27}$$

where $\psi_{R,\pm}(k)$ is the eigenstate of the corresponding Bloch Hamiltonian. We now wish to apply the same idea for NH systems. Previously, we saw that to obtain correct results in the OBC case from the PBC solutions, we need to apply a shift in k [see Eq. (25)]. Applying the same logic here, we make the following ansatz for the bulk eigenstates of the anisotropic SSH chain:

$$\tilde{\Psi}_{R,\pm}(k, n) = \frac{(t_1 - \gamma)^{n/2}}{(t_1 + \gamma)^{n/2}} e^{ikn}\tilde{\psi}_{R,\pm}(k), \tag{28}$$

where

$$\tilde{\psi}_{R,\pm}(k) = \begin{pmatrix} t_1 + \gamma + t_2\dfrac{\sqrt{t_1 + \gamma}}{\sqrt{t_1 - \gamma}}e^{-ik} \\ E_\pm^{\rm OBC}(k) \end{pmatrix}, \tag{29}$$

which we obtain by applying the shift in k in Eq. (22).

Next, we assume that all states have zero amplitude on the B sublattices $n = 0$ (or, equivalently, $n = 2N$) and $n = N$, as shown in Fig. 5. Upon cutting the chain open by removing the B sites at $n = 0$ ($n = 2N$) and $n = N$, we end up with two

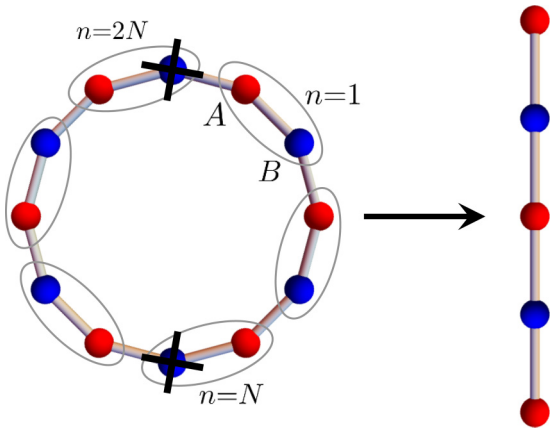

FIG. 5. Schematic picture of the periodic chain with A and B sublattices in red and blue, respectively, and the unit cells labeled by n depicted with gray ovals. Upon removing the B sublattices in unit cells $n = 0$ ($n = 2N$) and $n = N$, the periodic chain reduces to two open chains with A sublattices at their ends.

chains with N unit cells. In the following, we focus on one chain and imagine that we reattach the B sites at both ends. Using the spectral mirror symmetry of $E_{\pm}^{\mathrm{OBC}}(k) = E_{\pm}^{\mathrm{OBC}}(-k)$, we may write the bulk state in the nth unit cell as a superposition of $\tilde{\Psi}_{R,\pm}(k,n)$ and $\tilde{\Psi}_{R,\pm}(-k,n)$,

$$\begin{aligned}\Psi_{R,\mathrm{Bulk},\pm}(k,n) &= C_1\tilde{\Psi}_{R,\pm}(k,n) + C_2\tilde{\Psi}_{R,\pm}(-k,n)\\ &= \frac{(t_1-\gamma)^{n/2}}{(t_1+\gamma)^{n/2}}[C_1 e^{ikn}\tilde{\psi}_{R,\pm}(k) + C_2 e^{-ikn}\tilde{\psi}_{R,\pm}(-k)], \quad (30)\end{aligned}$$

where $k = \pi j/N$, with $j = 1, 2, \ldots, N-1$, and impose the boundary condition

$$\Psi_{R,\mathrm{Bulk},\pm,B}(k,0) = \Psi_{R,\mathrm{Bulk},\pm,B}(k,N) = 0, \quad (31)$$

where the label α in $\Psi_{R,\mathrm{Bulk},\pm,\alpha}(k,n)$ refers to the amplitude of $\Psi_{R,\mathrm{Bulk},\pm}(k,n)$ on sublattice α. The boundary condition leads to

$$\frac{C_2}{C_1} = -\frac{\tilde{\psi}_{R,\pm,B}(k)}{\tilde{\psi}_{R,\pm,B}(-k)} = -1, \quad (32)$$

such that

$$\begin{aligned}&\Psi_{R,\mathrm{Bulk},\pm,\alpha}(k,n)\\ &\quad= \frac{(t_1-\gamma)^{n/2}}{(t_1+\gamma)^{n/2}}[e^{ikn}\tilde{\psi}_{R,\pm,\alpha}(k) - e^{-ikn}\tilde{\psi}_{R,\pm,\alpha}(-k)]. \quad (33)\end{aligned}$$

We thus make the following ansatz for the (unnormalized) bulk states:

$$\Psi_{R,\mathrm{Bulk},\pm}(k) = \begin{pmatrix}\Psi_{R,\mathrm{Bulk},\pm,A}(k,1)\\ \Psi_{R,\mathrm{Bulk},\pm,B}(k,1)\\ \Psi_{R,\mathrm{Bulk},\pm,A}(k,2)\\ \Psi_{R,\mathrm{Bulk},\pm,B}(k,2)\\ \vdots\\ \Psi_{R,\mathrm{Bulk},\pm,B}(k,N-1)\\ \Psi_{R,\mathrm{Bulk},\pm,A}(k,N)\end{pmatrix}, \quad (34)$$

and a straightforward computation of the eigenequation, $H^{\mathrm{OBC}}\Psi_{R,\mathrm{Bulk},\pm}(k) = E_{\pm}^{\mathrm{OBC}}(k)\Psi_{R,\mathrm{Bulk},\pm}(k)$, shows that these are, indeed, eigenstates with energy $E_{\pm}^{\mathrm{OBC}}(k)$. The left eigenstates can be found by making use of the fact that the daggered Hamiltonian of the anisotropic SSH chain, i.e., $(H^{\mathrm{SSH}})^{\dagger}$, is simply obtained by transforming $\gamma \to -\gamma$ in the Hamiltonian H^{SSH}, such that these states are found by taking the complex conjugation of the right states and $\gamma \to -\gamma$, as shown in Appendix A.

We notice that Eq. (33) has two interesting features: First, we see that its weight explicitly depends on the unit-cell label n and the bulk sates are thus all localized to a boundary when $t_1, \gamma \neq 0$, while the states change localization when passing through $t_1 = 0$ and/or $\gamma = 0$.

Second, we notice that the bulk states [and also the shift in Eq. (25)] are singular when $t_1 = \pm\gamma$. From the Hamiltonian in Fig. 1(b), we immediately see that at these values of t_1 it is possible to hop in only one direction, and consequently, all eigenstates are exactly localized at the boundary. Additionally, the bulk spectrum has only two eigenvalues, $\pm t_2$ [see Eq. (26)]. This behavior of the eigenstates and eigenvalues is associated with the presence of EPs, and indeed, these points correspond to EPs with an order that scales with system size [38]. The bulk states thus merge into two different states as they approach one of the EPs.

A natural question is, What happens with the bulk-state solution in Eq. (33) at these points? We note that an eigenvector of an operator is determined only up to multiplication by a scalar, and we show in Appendix B that we can choose a scalar in such a way that the limit $t_1 \to \pm\gamma$ exists. We note these multiplicative factors differ for the two EPs. We then find that the right and left eigenstates have only nonzero amplitudes at opposite boundaries [e.g., Eqs. (B5), (B6), (B9), and (B10)], which means that the states are not normalizable, which is consistent with the behavior of an EP.

C. Twisted states

We will now elucidate and provide physical intuition by comparing the boundary state to approximate variational states. We do this by studying what happens with the bulk states at the gap closings in the spectrum, i.e., at $|r_R r_L| = 1$. To gain further understanding of this, we normalize the bulk states found in the previous section for $|t_1| > |\gamma|$ and $t_1 + \gamma > 0$ at the point $t_2 = \sqrt{t_1^2 - \gamma^2}$,

$$\langle\Psi_{L,\mathrm{Bulk},\pm}|\Psi_{R,\mathrm{Bulk},\pm}\rangle = -16N(t_1^2-\gamma^2)\cos^2\left(\frac{k}{2}\right), \quad (35)$$

such that the normalized state takes the form

$$|\Psi_{R,\mathrm{Bulk},\pm}(k)\rangle = |\Psi_{\mathrm{twist},A}(k)\rangle \pm |\Psi_{\mathrm{twist},B}(k)\rangle, \quad (36)$$

where

$$\begin{aligned}|\Psi_{\mathrm{twist},A}(k)\rangle = \frac{1}{\sqrt{N}}\sum_{n=1}^{N}\left(\frac{t_1-\gamma}{t_2}\right)^{n-1}\\ \times \sin\left(\frac{(2n-1)k}{2}\right)c_{n,A}^{\dagger}|0\rangle \quad (37)\end{aligned}$$

and

$$|\Psi_{\mathrm{twist},B}(k)\rangle = \frac{1}{\sqrt{N}}\sum_{n=1}^{N-1}\left(\frac{t_1-\gamma}{t_2}\right)^{n}\sin(nk)c_{n,B}^{\dagger}|0\rangle. \quad (38)$$

We note these states are *twisted* versions of the eigenstates of the zero-energy mode in Eq. (24) in the sense that while they have the same amplitude, they also feature an additional phase that changes along the chain. Indeed, the larger the length of the chain is, the smaller the local twist becomes. This means that in the limit of going to infinite system size, the twisted state has the same energy as the zero-energy state, and they are thus degenerate. Therefore, the bulk-band gap must close when $t_2 = \sqrt{t_1^2 - \gamma^2}$. We repeat this calculation for $|t_1| < |\gamma|$ and $\gamma + t_1 > 0$ at the point $t_2 = \sqrt{\gamma^2 - t_1^2}$ in Appendix C and show that we arrive at the same conclusion.

IV. DISCUSSION

In this paper, we have further expanded the toolbox of methods for characterizing and finding analytical solutions in NH systems. Specifically, we generalized the biorthogonal polarization $\mathcal{P}$ first proposed in Ref. [30] to be applicable to quasi-one-dimensional systems with any number of boundary modes. Crucially, we showed that this generalization is applicable to models that cannot be described as copies of a single system. We showed that $\mathcal{P}$ is gauge invariant, which is a crucial property for measurable quantities. Additionally, we showed that $\mathcal{P}$ is invariant under local unitary transformations. As a consequence, the biorthogonal polarizations for models that are related via the same unitary transformation are thus equivalent. We emphasize that even though we explicitly treated one-dimensional examples to study the generalized biorthogonal polarization, the formalism developed in this paper works for any model with boundaries of codimension 1, i.e., for any d-dimensional system with boundaries of $d-1$ dimensions. Moreover, we believe that the generalized biorthogonal polarization should be readily further generalizable to systems with boundaries of higher codimension. Indeed, in Ref. [31], the quantity $\langle\psi_L|\Pi_{n,n',\ldots}|\psi_R\rangle$, with $n, n', \ldots$ labeling the unit cells in the different directions, was shown to accurately capture the presence of corner and hinge states for lattice models with OBCs in more directions.

We also studied the anisotropic SSH chain in Fig. 1(b) in great detail. By making use of a shift in k that connects the PBC and OBC cases to each other [see Eq. (25)], it is possible to find analytical expressions for the eigenvalues as already presented in Ref. [38]. Making use of these solutions for the OBC case, we showed that the finite-size gaps may close slowly in NH systems compared to Hermitian ones. In particular, we find $E_{\text{gap}} \propto N^{-1/p}$, while gap closings in the Brillouin zone may scale as $E_{\text{gap}} \propto (k - k_0)^{1/p}$, with p being some integer. These gap closings are sharper than those in Hermitian systems, which remain analytic. While we focus on two-band models in this work, where $p \leqslant 2$, this type of scaling is expected to persist once more bands are considered. In this context we note, however, that two-band models are sufficient to study (ordinary) band crossings as these generically occur in a three-dimensional parameter space and that models with band crossings involving more bands generically require the tuning of a large number of parameters.

By extending the method in Ref. [69] and making use of the shift in Eq. (25), we were able to not only find the eigenvalues but also find closed-form analytical equations for all bulk states for the anisotropic SSH model with OBCs in addition to the end state solutions that were already found in Ref. [30]. Making use of these solutions, we were able to prove that the band gap indeed closes when $|r_R r_L| = 1$ [69]. While we here showed only that this method works for a specific example, the anisotropic SSH chain, we believe that it should be applicable to a large family of quasi-one-dimensional NH lattice models with $E^{\text{OBC}}(k_\perp, \mathbf{k}_\parallel) = E^{\text{OBC}}(-k_\perp, \mathbf{k}_\parallel)$, in analogy to the Hermitian version of this approach [69].

Our analytical results complement a large body of recent numerical and experimental studies on non-Hermitian systems and offer as such complementary and detailed insights into an active field of contemporary and cross-disciplinary physics.

ACKNOWLEDGMENTS

E.E., F.K.K., and E.J.B. acknowledge useful discussions with J. Budich and G. van Miert on related projects. We used the MATLAB extension ADVANPIX to produce the plot for the polarization. E.E. and E.J.B. are funded by the Swedish Research Council (VR) and the Knut and Alice Wallenberg Foundation. F.K.K. is supported by the Max Planck Institute of Quantum Optics (MPQ) and the Max-Planck-Harvard Research Center for Quantum Optics (MPHQ). T.Y. was supported in part by JSPS KAKENHI Grant No. JP20H04627.

APPENDIX A: RELATION BETWEEN THE RIGHT AND LEFT EIGENSTATES

Here, we show that in a system with open boundary conditions, we can find the left eigenstates from the right eigenstates by using the fact that the Hamiltonian is symmetric under Hermitian conjugation and $\gamma \mapsto -\gamma$. Therefore, the left eigenstates are given by the complex-conjugated right eigenstates with mirrored γ. To see this, suppose that

$$H(\gamma)\big|\psi_R^n(\gamma)\big\rangle = E_n(\gamma)\big|\psi_R^n(\gamma)\big\rangle. \tag{A1}$$

We wish to find the corresponding left eigenstate $|\psi_L^n(\gamma)\rangle$, which we know satisfies

$$H^\dagger(\gamma)\big|\psi_L^n(\gamma)\big\rangle = E_n^*\big|\psi_L^n(\gamma)\big\rangle. \tag{A2}$$

Complex conjugating this equation, letting $\gamma \mapsto -\gamma$, and using that we know that $H^\dagger(-\gamma) = H^T(-\gamma) = H(\gamma)$ and that Eq. (26) gives us $E_n(-\gamma) = E_n(\gamma)$, we get

$$H(\gamma)\big|\psi_L^n(-\gamma)\big\rangle^* = E_n(\gamma)\big|\psi_L^n(-\gamma)\big\rangle^*, \tag{A3}$$

and we get

$$\big|\psi_L^n(\gamma)\big\rangle = \big|\psi_R^n(-\gamma)\big\rangle^*. \tag{A4}$$

For the Bloch Hamiltonian, a slightly different argument must be used as it not symmetric under Hermitian conjugation and $\gamma \mapsto -\gamma$ separately, but rather under the composition of those. For periodic boundary conditions, we also have $E(k, \gamma) = E^*(k, -\gamma)$, in contrast to the case for open boundary conditions. The equation for the left eigenstates of the Bloch Hamiltonian is given by

$$H_{\text{Bloch}}^\dagger(k, \gamma)|\psi_L(k, \gamma)\rangle = E^*(k, \gamma)|\psi_L(k, \gamma)\rangle. \tag{A5}$$

Letting $\gamma \mapsto -\gamma$, we get

$$H^{\dagger}_{\mathrm{Bloch}}(k,-\gamma)|\psi_L(k,-\gamma)\rangle = E^*(k,-\gamma)|\psi_L(k,-\gamma)\rangle, \quad \text{(A6)}$$

which implies

$$H_{\mathrm{Bloch}}(k,\gamma)|\psi_L(k,-\gamma)\rangle = E(k,\gamma)|\psi_L(k,-\gamma)\rangle, \quad \text{(A7)}$$

such that

$$|\psi_L(k,\gamma)\rangle = |\psi_R(k,-\gamma)\rangle. \quad \text{(A8)}$$

APPENDIX B: BULK STATES AT THE EXCEPTIONAL POINTS

We study what happens when we approach the exceptional point at $t_1 = \gamma > 0$ from $t_1 > \gamma$. We see that if the right eigenstates in Eq. (33) are multiplied by

$$\frac{\sqrt{t_1+\gamma}}{\sqrt{t_1-\gamma}}\frac{1}{\sin(k)} \quad \text{(B1)}$$

and the left eigenstates are multiplied by

$$\frac{(t_1-\gamma)^{(N-1)/2}}{(t_1+\gamma)^{(N-1)/2}}\frac{1}{\sin[k(N-1)]}, \quad \text{(B2)}$$

we find

$$\Psi_{R,\mathrm{Bulk},\pm,A}(k,n) = 2i\frac{(t_1-\gamma)^{(n-1)/2}}{(t_1+\gamma)^{(n-1)/2}} \times\left[(t_1+\gamma)\frac{\sin(kn)}{\sin(k)} + t_2\frac{\sqrt{t_1+\gamma}}{\sqrt{t_1-\gamma}}\frac{\sin[k(n-1)]}{\sin(k)}\right] \quad \text{(B3)}$$

and

$$\Psi_{R,\mathrm{Bulk},\pm,B}(k,n) = 2i\frac{(t_1-\gamma)^{(n-1)/2}}{(t_1+\gamma)^{(n-1)/2}}E^{\mathrm{OBC}}_{\pm}(k)\frac{\sin(kn)}{\sin(k)}. \quad \text{(B4)}$$

We see that

$$\lim_{t_1\to\gamma}\Psi_{R,\mathrm{Bulk},\pm,A}(k,n) = \begin{cases} 4i\gamma & \text{if } n=1,\\ 2it_2 & \text{if } n=2,\\ 0 & \text{if } n>2,\end{cases} \quad \text{(B5)}$$

and

$$\lim_{t_1\to\gamma}\Psi_{R,\mathrm{Bulk},\pm,B}(k,n) = \begin{cases} \pm 2it_2 & \text{if } n=1,\\ 0 & \text{if } n>1.\end{cases} \quad \text{(B6)}$$

In a similar fashion, the corresponding left eigenstates, after multiplication by the appropriate factor, are given by

$$\Psi_{L,\mathrm{Bulk},\pm,A}(k,n) = -2i\frac{(t_1-\gamma)^{(N-n-1)/2}}{(t_1+\gamma)^{(N-n-1)/2}} \times\left[(t_1-\gamma)\frac{\sin(kn)}{\sin[k(N-1)]} + t_2\frac{\sqrt{t_1-\gamma}}{\sqrt{t_1+\gamma}}\frac{\sin[k(n-1)]}{\sin[k(N-1)]}\right] \quad \text{(B7)}$$

and

$$\Psi_{L,\mathrm{Bulk},\pm,B}(k,n) = -2i\frac{(t_1-\gamma)^{(N-n-1)/2}}{(t_1+\gamma)^{(N-n-1)/2}} \times E^{\mathrm{OBC}}_{\pm}(k)\frac{\sin(kn)}{\sin[k(N-1)]}, \quad \text{(B8)}$$

and we get

$$\lim_{t_1\to\gamma}\Psi_{L,\mathrm{Bulk},\pm,A}(k,n) = \begin{cases} -2it_2 & \text{if } n=N,\\ 0 & \text{if } n<N,\end{cases} \quad \text{(B9)}$$

and

$$\lim_{t_1\to\gamma}\Psi_{L,\mathrm{Bulk},\pm,B}(k,n) = \begin{cases} \mp 2it_2 & \text{if } n=N-1,\\ 0 & \text{if } n<N-1.\end{cases} \quad \text{(B10)}$$

We note that we need to pick different prefactors for the eigenstates in order for them to approach the correct states at the other EP at $t_1 = -\gamma$ but that a similar solution would be found with the difference that the right and left eigenstates are now localized to the opposite boundaries.

APPENDIX C: TWISTED STATES

For $|\gamma| > |t_1|$ and $t_1 + \gamma > 0$ at the point $t_2 = \sqrt{\gamma^2 - t_1^2}$, we instead get

$$\langle\Psi_{L,\mathrm{Bulk},\pm}|\Psi_{R,\mathrm{Bulk},\pm}\rangle = 8iN\left(t_1^2-\gamma^2\right)\cos(k). \quad \text{(C1)}$$

We again get

$$|\Psi_{R,\mathrm{Bulk},\pm}(k)\rangle = |\Psi_{\mathrm{twist},A}(k)\rangle \pm |\Psi_{\mathrm{twist},B}(k)\rangle, \quad \text{(C2)}$$

but in this case, we have

$$|\Psi_{\mathrm{twist},A}(k)\rangle = -\frac{1}{\sqrt{N}}\frac{1}{\sqrt{-2i\cos(k)}} \times\sum_{n=1}^{N}\frac{1}{i^{n-1}}\left(\frac{t_1-\gamma}{t_2}\right)^{n-1}\{\sin(kn) - i\sin[k(n-1)]\}c^{\dagger}_{n,A}|0\rangle \quad \text{(C3)}$$

and

$$|\Psi_{\mathrm{twist},B}(k)\rangle = -\frac{1}{\sqrt{N}}\frac{|\cos(k)|}{\cos(k)}\sum_{n=1}^{N-1}(-i)^n\left(\frac{t_1-\gamma}{t_2}\right)^n\sin(nk)c^{\dagger}_{n,B}|0\rangle. \quad \text{(C4)}$$

The states are not as nice as in the point $t_2^2 = t_1^2 - \gamma^2$, but one can still see that they are sums of trigonometric functions that one can interpret as a slow change in phase.

[1] A. Szameit, M. C. Rechtsman, O. Bahat-Treidel, and M. Segev, PT-symmetry in honeycomb photonic lattices, Phys. Rev. A **84**, 021806(R) (2011).

[2] A. Regensburger, C. Bersch, M. Miri, G. Onishchukov, D. N. Christodoulides, and U. Peschel, Parity-time synthetic photonic lattices, Nature (London) **488**, 167 (2012).

[3] J. Wiersig, Enhancing the Sensitivity of Frequency and Energy Splitting Detection by Using Exceptional Points: Application to Microcavity Sensors for Single-Particle Detection, Phys. Rev. Lett. **112**, 203901 (2014).

[4] H. Hodaei, A. U. Hassan, S. Wittek, H. Garcia-Gracia, R. El-Ganainy, D. N. Christodoulides, and M. Khajavikhan, Enhanced sensitivity at higher-order exceptional points, Nature (London) **548**, 187 (2017).

[5] L. Feng, R. El-Ganainy, and L. Ge, Non-Hermitian photonics based on parity-time symmetry, Nat. Photonics **11**, 752 (2017).

[6] D. L. Sounas and A. Alù, Non-reciprocal photonics based on time modulation, Nat. Photonics **11**, 774 (2017).

[7] G. Harari, M. A. Bandres, Y. Lumer, M. C. Rechtsman, Y. D. Chong, M. Khajavikhan, D. N. Christodoulides, and M. Segev, Topological insulator laser: Theory, Science **359**, eaar4003 (2018).

[8] M. A. Bandres, S. Wittek, G. Harari, M. Parto, J. Ren, M. Segev, D. N. Christodoulides, and M. Khajavikhan, Topological insulator laser: Experiments, Science **359**, eaar4005 (2018).

[9] H. Zhao, P. Miao, M. H. Teimourpour, S. Malzard, R. El-Ganainy, H. Schomerus, and L. Feng, Topological hybrid silicon microlasers, Nat. Commun. **9**, 981 (2018).

[10] M. Kremer, T. Biesenthal, L. J. Maczewsky, M. Heinrich, R. Thomale, and A. Szameit, Demonstration of a two-dimensional PT-symmetric crystal, Nat. Commun. **10**, 435 (2019).

[11] S. K. Özdemir, S. Rotter, F. Nori, and L. Yang, Parity–time symmetry and exceptional points in photonics, Nat. Mater. **18**, 783 (2019).

[12] J. Ningyuan, C. Owens, A. Sommer, D. Schuster, and J. Simon, Time- and Site-Resolved Dynamics in a Topological Circuit, Phys. Rev. X **5**, 021031 (2015).

[13] V. V. Albert, L. I. Glazman, and L. Jiang, Topological Properties of Linear Circuit Lattices, Phys. Rev. Lett. **114**, 173902 (2015).

[14] C. H. Lee, S. Imhof, C. Berger, F. Bayer, J. Brehm, L. W. Molenkamp, T. Kiessling, and R. Thomale, Topoelectrical circuits, Commun. Phys. **1**, 39 (2018).

[15] M. Ezawa, Non-Hermitian higher-order topological states in nonreciprocal and reciprocal systems with their electric-circuit realization, Phys. Rev. B **99**, 201411(R) (2019).

[16] T. Helbig, T. Hofmann, S. Imhof, M. Abdelghany, T. Kiessling, L. W. Molenkamp, C. H. Lee, A. Szameit, M. Greiter, and R. Thomale, Generalized bulkboundary correspondence in non-Hermitian topolectrical circuits, Nat. Phys. **16**, 747 (2020).

[17] T. Hofmann, T. Helbig, F. Schindler, N. Salgo, M. Brzezińska, M. Greiter, T. Kiessling, D. Wolf, A. Vollhardt, A. Kabaši, C. H. Lee, A. Bilušić, R. Thomale, and T. Neupert, Reciprocal skin effect and its realization in a topolectrical circuit, Phys. Rev. Research **2**, 023265 (2020).

[18] T. Yoshida, T. Mizoguchi, and Y. Hatsugai, Mirror skin effect and its electric circuit simulation, Phys. Rev. Res. **2**, 022062(R) (2020).

[19] L. M. Nash, D. Kleckner, A. Read, V. Vitelli, A. M. Turner, and W. T. M. Irvine, Topological mechanics of gyroscopic metamaterials, Proc. Natl. Acad. Sci. USA **112**, 14495 (2015).

[20] M. Brandenbourger, X. Locsin, E. Lerner, and C. Coulais, Non-reciprocal robotic metamaterials, Nat. Comm. **10**, 4608 (2019).

[21] A. Ghatak, M. Brandenbourger, J. van Wezel, and C. Coulais, Observation of non-Hermitian topology and its bulk-edge correspondence, arXiv:1907.11619.

[22] T. Yoshida and Y. Hatsugai, Exceptional rings protected by emergent symmetry for mechanical systems, Phys. Rev. B **100**, 054109 (2019).

[23] V. Kozii and L. Fu, Non-Hermitian Topological Theory of Finite-lifetime quasiparticles: Prediction of bulk fermi arc due to exceptional point, arXiv:1708.05841.

[24] T. Yoshida, R. Peters, and N. Kawakami, Non-Hermitian perspective of the band structure in heavy-fermion systems, Phys. Rev. B **98**, 035141 (2018).

[25] T. Yoshida, R. Peters, N. Kawakami, and Y. Hatsugai, Exceptional band touching for strongly correlated systems in equilibrium, Prog. Theor. Exp. Phys. ptaa059 (2020).

[26] E. J. Bergholtz and J. C. Budich, Non-Hermitian Weyl physics in topological insulator ferromagnet junctions, Phys. Rev. Res. **1**, 012003(R) (2019).

[27] E. J. Bergholtz, J. C. Budich, and F. K. Kunst, Exceptional topology of non-Hermitian systems, arXiv:1912.10048.

[28] K. Kawabata, T. Bessho, and M. Sato, Classification of Exceptional Points and Non-Hermitian Topological Semimetals, Phys. Rev. Lett. **123**, 066405 (2019).

[29] C. H. Lee, L. Li, and J. Gong, Hybrid Higher-Order Skin-Topological Modes in Nonreciprocal Systems, Phys. Rev. Lett. **123**, 016805 (2019).

[30] F. K. Kunst, E. Edvardsson, J. C. Budich, and E. J. Bergholtz, Biorthogonal Bulk-Boundary Correspondence in Non-Hermitian Systems, Phys. Rev. Lett. **121**, 026808 (2018).

[31] E. Edvardsson, F. K. Kunst, E. J. Bergholtz, Non-Hermitian extensions of higher-order topological phases and their biorthogonal bulk-boundary correspondence, Phys. Rev. B **99**, 081302(R) (2019).

[32] R. Koch and J. C. Budich, Bulk-boundary correspondence in non-Hermitian systems: Stability analysis for generalized boundary conditions, Eur. Phys. J. D **74**, 70 (2020).

[33] V. M. Martinez Alvarez, J. E. Barrios Vargas, and L. E. F. Foa Torres, Non-Hermitian robust edge states in one dimension: Anomalous localization and eigenspace condensation at exceptional points, Phys. Rev. B **97**, 121401(R) (2018).

[34] Y. Xiong, Why does bulk boundary correspondence fail in some non-Hermitian topological models, J. Phys. Commun. **2**, 035043 (2018).

[35] T. E. Lee, Anomalous edge state in a non-Hermitian lattice, Phys. Rev. Lett **116**, 133903 (2016).

[36] Y. Xiong, T. Wang, X. Wang, and P. Tong, Comment on "Anomalous edge state in a non-Hermitian lattice," arXiv:1610.06275.

[37] S. Yao and Z. Wang, Edge States and Topological Invariants of Non-Hermitian Systems, Phys. Rev. Lett. **121**, 086803 (2018).

[38] F. K. Kunst and V. Dwivedi, Non-Hermitian systems and topology: A transfer-matrix perspective, Phys. Rev. B **99**, 245116 (2019).

[39] J. Carlström, M. Stålhammar, J. C. Budich, and E. J. Bergholtz, Knotted non-Hermitian metals, Phys. Rev. B **99**, 161115(R) (2019).

[40] J. C. Budich, J. Carlström, F. K. Kunst, and E. J. Bergholtz, Symmetry-protected nodal phases in non-Hermitian systems, Phys. Rev. B **99**, 041406(R) (2019).

[41] T. Yoshida, R. Peters, N. Kawakami, and Y. Hatsugai, Symmetry-protected exceptional rings in two-dimensional correlated systems with chiral symmetry, Phys. Rev. B **99**, 121101(R) (2019).

[42] J. Carlström and E. J. Bergholtz, Exceptional links and twisted Fermi ribbons in non-Hermitian systems, Phys. Rev. A **98**, 042114 (2018).

[43] Z. Gong, Y. Ashida, K. Kawabata, K. Takasan, S. Higashikawa, and M. Ueda, Topological Phases of Non-Hermitian Systems, Phys. Rev. X **8**, 031079 (2018).

[44] H. Zhou and J. Y. Lee, Periodic table for topological bands with non-Hermitian symmetries, Phys. Rev. B **99**, 235112 (2019).

[45] M. Stålhammar, L. Rødland, G. Arone, J. C. Budich, and E. J. Bergholtz, Hyperbolic nodal band structures and knot invariants, SciPost Phys. **7**, 019 (2019).

[46] D. Leykam, K. Y. Bliokh, C. Huang, Y. D. Chong, and F. Nori, Edge Modes, Degeneracies, and Topological Numbers in Non-Hermitian Systems, Phys. Rev. Lett. **118**, 040401 (2017).

[47] H. Shen, B. Zhen, and L. Fu, Topological Band Theory for Non-Hermitian Hamiltonians, Phys. Rev. Lett. **120**, 146402 (2018).

[48] D. J. Luitz and F. Piazza, Exceptional points and the topology of quantum many-body spectra, Phys. Rev. Res. **1**, 033051 (2019).

[49] K. Kawabata, K. Shiozaki, M. Ueda, and M. Sato, Symmetry and Topology in Non-Hermitian Physics, Phys. Rev. X **9**, 041015 (2019).

[50] X.-W. Luo and C. Zhang, Higher-Order Topological Corner States Induced by Gain and Loss, Phys. Rev. Lett. **123**, 073601 (2019).

[51] F. Terrier and F. K. Kunst, Dissipative analog of four-dimensional quantum Hall physics, Phys. Rev. Res. **2**, 023364 (2020).

[52] K. Esaki, M. Sato, K. Hasebe, and M. Kohmoto, Edge states and topological phases in non-Hermitian systems, Phys. Rev. B **84**, 205128 (2011).

[53] T. Yoshida, K. Kudo, and Y. Hatsugai, Non-Hermitian fractional quantum Hall states, Sci. Rep. **9**, 16895 (2019).

[54] T. Yoshida, K. Kudo, H. Katsura, and Y. Hatsugai, Fate of fractional quantum Hall states in open quantum systems: Characterization of correlated topological states for the full Liouvillian, Phys. Rev. Res. **2**, 033428 (2020).

[55] Z. Wang, Y. Chong, J. D. Joannopoulos, and M. Soljačić, Observation of unidirectional backscattering-immune topological electromagnetic states, Nature (London) **461**, 772 (2009).

[56] J. M. Zeuner, M. C. Rechtsman, Y. Plotnik, Y. Lumer, S. Nolte, M. S. Rudner, M. Segev, and A. Szameit, Observation of a Topological Transition in the Bulk of a Non-Hermitian System, Phys. Rev. Lett. **115**, 040402 (2015).

[57] B. Peng, Ş. K. Özdemir, M. Liertzer, W. Chen, J. Kramer, H. Yılmaz, J. Wiersig, S. Rotter, and L. Yang, Chiral modes and directional lasing at exceptional points, Proc. Natl. Acad. Sci. USA **113**, 6845 (2016).

[58] S. Weimann, M. Kremer, Y. Plotnik, Y. Lumer, S. Nolte, K. G. Makris, M. Segev, M. C. Rechtsman, and A. Szameit, Topologically protected bound states in photonic parity-time-symmetric crystals, Nat. Mater. **16**, 433 (2017).

[59] W. Chen, Ş. K. Özdemir, G. Zhao, J. Wiersig, and L. Yang, Exceptional points enhance sensing in an optical microcavity, Nature (London) **548**, 192 (2017).

[60] A. Cerjan, S. Huang, M. Wang, K. P. Chen, Y. Chong, and M. C. Rechtsman, Experimental realization of a Weyl exceptional ring, Nat. Photonics **13**, 623 (2019).

[61] L. Xiao, T. Deng, K. Wang, G. Zhu, Z. Wang, W. Yi, and P. Xue, Non-Hermitian bulk–boundary correspondence in quantum dynamics, Nat. Phys. **16**, 761 (2020).

[62] H. He, C. Qiu, L. Ye, X. Cai, X. Fan, M. Ke, F. Zhang, and Z. Liu, Topological negative refraction of surface acoustic waves in a Weyl phononic crystal, Nature (London) **560**, 61 (2018).

[63] H. Zhou, C. Peng, Y. Yoon, C. W. Hsu, K. A. Nelson, L. Fu, J. D. Joannopoulos, M. Soljačić, and B. Zhen, Observation of bulk Fermi arc and polarization half charge from paired exceptional points, Science **359**, 1009 (2018).

[64] H. Zhou, J. Y. Lee, S. Liu, and B. Zhen, Exceptional surfaces in PT-symmetric non-Hermitian photonic systems, Optica **6**, 190 (2019).

[65] C. Poli, M. Bellec, U. Kuhl, F. Mortessagne, and H. Schomerus, Selective enhancement of topologically induced interface states in a dielectric resonator chain, Nat. Commun. **6**, 6710 (2015).

[66] J. C. Budich and E. J. Bergholtz, Non-Hermitian topological sensors, arXiv:2003.13699.

[67] D. C. Brody, Biorthogonal quantum mechanics, J. Phys. A **47**, 035305 (2013).

[68] A. G. Rojo, Absence of gap for infinite half-integer spin ladders with an odd number of legs, Phys. Rev. B **53**, 9172 (1996).

[69] F. K. Kunst, G. van Miert, and E. J. Bergholtz, Extended Bloch theorem for topological lattice models with open boundaries, Phys. Rev. B **99**, 085427 (2019).

[70] Generally, models that terminate with the same sublattice(s) on both ends feature a boundary state that always exists regardless of the choice of parameters, see, e.g., Ref. [69] and references therein.